Nanoparticle Engineering of Complex Fluid Behavior

Valeria Tohver,[†] Angel Chan,[†] Osamu Sakurada,[†] and Jennifer A. Lewis*[,‡,§,⊥]

Materials Science and Engineering Department, Chemical Engineering Department, and Beckman Institute for Advanced Science and Technology, University of Illinois at Urbana-Champaign, Urbana, Illinois 61801

Received August 7, 2001. In Final Form: September 18, 2001

A new mechanism for regulating the stability of colloidal suspensions has been discovered, known as nanoparticle haloing.[1] Colloidal microspheres suspended under conditions near their isoelectric point were stabilized by the addition of highly charged nanoparticles. Such species segregated to regions near negligibly charged microspheres leading to their effective charge buildup. At even higher nanoparticle volume fractions, system stability was reversed due to attractive depletion interactions. By engineering the strength of energetic and entropic interactions via nanoparticle additions, we have assembled colloidal fluid, gel, and crystalline phases from binary mixtures of colloidal silica microspheres and hydrous zirconia nanoparticles whose structure and flow behavior vary dramatically.

Introduction

Complex fluids enjoy widespread use in applications ranging from advanced materials to drug delivery. By tailoring interactions between colloidal particles suspended in the fluid phase, one can design systems that serve as feedstock for ceramics processing,[2] coatings,[3] direct write technologies,[4,5] and photonic[6−11] and pharmaceutical[12] materials. Long-range, attractive van der Waals forces are ubiquitous and therefore must be balanced by Coulombic, steric, or other repulsive interactions to control their behavior. Nanoparticle engineering is a new paradigm by which such interactions may be regulated.

Despite their broad importance, the transitions between, and structure of, the fluid, gel, crystalline, and glassy states have been primarily studied in hard-sphere systems that interact only through infinite repulsion on contact.[13−17] Binary mixtures of hard-sphere colloids exhibit a rich phase behavior that depends on three dimensionless parameters: the volume fractions of large (ϕ_L) and small (ϕ_S) spheres, respectively, and their radii ratio (a_L/a_S).[13−15] In such systems, entropic forces are solely responsible for the observed phase behavior. The term "depletion" describes the exclusion of smaller species from the gap region between colloidal particles that arises when their separation distance becomes less than the characteristic depletant size. The resulting concentration gradient between the gap region and bulk solution gives rise to an attractive force at low ϕ_L, whose magnitude scales with the volume fraction of smaller species and the size ratio of large to small species.[18,19] At higher ϕ_L and/or ϕ_S, liquid packing effects can result in a decaying oscillatory force that includes both attractive minima and repulsive maxima, whose periodicity coincides with the characteristic depletant size.[20,21]

Imhof and Dhont[14] systematically studied hard sphere mixtures of silica (a_L = 365 nm)/silica (a_S = 39 nm) suspended in an index-matched solvent system of *N*,*N*-dimethylformamide (DMF) with 0.01 M LiCl. In the absence of smaller silica spheres, the large ones exhibited fluid behavior at $\phi_L < 0.49$, a fluid-crystal coexistence region from $0.49 \leq \phi_L < 0.54$, and fully crystallized at $\phi_L \geq 0.54$. Upon the addition of smaller silica spheres, they found that the fluid−crystal coexistence region broadened for mixtures of large ϕ_L and small ϕ_S. At intermediate concentrations, an attractive depletion force induced gelation of the large spheres. This gel phase was found to be in equilibrium with either a fluid phase or a gel phase consisting of smaller silica spheres depending on ϕ_S.

Unlike hard-sphere binary mixtures[13−15] whose phase behavior is driven solely by entropic effects, energetic considerations must be included for more complex mixtures, such as the microsphere−nanoparticle systems studied here. The presence of van der Waals and/or electrostatic forces allow colloidal species to interact over much longer distances than the short-range, excluded volume interactions experienced by hard spheres. This important qualitative difference can profoundly influence their behavior.

[†] Materials Science and Engineering Department.
[‡] Chemical Engineering Department.
[§] Beckman Institute for Advanced Science and Technology.
[⊥] Frederick Seitz Materials Research Laboratory.

(1) Tohver, V.; Smay, J. E.; Braem, A.; Braun, P. V.; Lewis, J. A. *Proc. Natl. Acad. Sci. U.S.A.* **2001**, *98* (16), 8950−8954.
(2) Lewis, J. A. *J. Am. Ceram. Soc.* **2000**, *83*, 3241−3259.
(3) Agarwal, N.; Farris, R. J. *Polym. Eng. Sci.* **2000**, *40*, 376−390.
(4) Chrisey, D. B. *Science* **2000**, *289*, 879−881.
(5) Smay, J. E.; Cesarano, J.; Lewis, J. A. *Adv. Mater.*, submitted for publication.
(6) Yablonovitch, E. *Phys. Rev. Lett.* **1987**, *58*, 2059−2062.
(7) Joannopoulos, J. D.; Villeneuve, P. R.; Fan, S. *Nature* **1997**, *386*, 143−149.
(8) Braun, P. V.; Wiltzius, P. *Nature* **1999**, *402*, 603−604.
(9) Pan, G.; Kesavamoorthy, R.; Asher, S. A. *Phys. Rev. Lett.* **1997**, *78*, 3860−3863.
(10) Johnson, S. A.; Olivier, P. J.; Mallouk, T. E. *Science* **1999**, *283*, 963−965.
(11) Burmeister, F.; Schäfle, C.; Matthes, T.; Böhmisch, M.; Boneberg, J.; Leiderer, P. *Langmuir* **1997**, *13*, 2983−2987.
(12) Muller, R. H. In *Colloidal Carriers for Controlled Drug Delivery and Targeting: Modification, Characterization, and In Vivo Distribution*; CRC Press: Boca Raton, FL, 1991.
(13) Biben, T.; Hansen, J.-P. *Phys. Rev. Lett.* **1991**, *66*, 2215−2218.
(14) Imhof, A.; Dhont, J. K. G. *Phys. Rev. Lett.* **1995**, *75*, 1662−1665.
(15) Dinsmore, A. D.; Yodh, A. G.; Pine, D. J. *Phys. Rev. E* **1995**, *52*, 4045−4057.
(16) Kaplan, P. D.; Rouke, J. L.; Yodh, A. G.; Pine, A. J. *Phys. Rev. Lett.* **1994**, *72*, 582−585.
(17) Bartlett, P.; Ottewill, R. H.; Pusey, P. N. *Phys. Rev. Lett.* **1992**, *68*, 3801−3804.
(18) Oosawa, F.; Asakura, S. *J. Chem. Phys.* **1954**, *22*, 1255−56.
(19) Asakura, S.; Oosawa, F. *J. Polym. Sci.* **1958**, *33*, 183−192.
(20) Mao, Y.; Cates, M. E.; Lekkerkerker, H. N. W. *Physica A* **1995**, *222*, 10−24.
(21) Walz, J. Y.; Sharma, A. *J. Colloid Interface Sci.* **1994**, *168*, 485−496.

10.1021/la011252w CCC: $20.00
Published on Web 11/20/2001

The self-organization of highly charged nanoparticles and their effects on complex fluids in which they dwell have received scant attention. Emerging theoretical work[22−24] predicts that charged nanoparticles in solution may influence system stability by segregating to regions near large *uncharged* colloids, especially in systems with high size asymmetry and many more small to large spheres.[22] This type of segregation can be driven solely by Coulombic repulsions between smaller species in solution and occurs simply because the larger particles represent a big volume without charge. We have recently shown that nanoparticle haloing gives rise to a new mechanism for regulating the effective charge and, hence, stability of colloidal particles.[1]

Here, we study the effects of highly charged nanoparticles on the phase behavior, structure, and rheological properties of colloidal microsphere−nanoparticle mixtures, which undergo a remarkable transition from a colloidal gel → stable fluid → colloidal gel with increasing nanoparticle additions. We attribute the stabilizing transition to nanoparticle haloing around the microspheres, which serves to mitigate their long-range van der Waals attraction. The system stability is ultimately reversed at higher nanoparticle volume fractions, where flocculation ensues due to entropic depletion forces. With the balance of energetic and entropic forces in this intermediary concentration range, microsphere colloidal crystals could be assembled from the homogeneous fluid mixture via gravity-driven sedimentation. By exploiting this unique stabilizing mechanism, we offer a novel route for producing colloidal gels of varying strength for directed assembly routes[2,5] as well as robust, periodic colloidal structures required for photonic crystals, including band gap,[6−8] optical switching,[9] mesoporous,[10] and lithographic[11] materials.

Experimental Section

Materials System. Uniform silica microspheres (Geltech, Alachua, FL) served as the large colloidal species. The microspheres have an average radius, a_{micro}, of 0.285 ± 0.01 or 0.590 ± 0.01 μm, as determined from quantitive image analysis carried out on scanning electron microscopy (SEM) photomicrographs (15000× magnification), and a density of 2.25 g/cm^3, as determined by helium pycnometry (model AccuPyc 1330, Micromeritics Instrument Corp., Norcross, GA). They exhibited an isoelectric point at pH ∼ 2.5 and a zeta potential of approximately 1 mV at pH = 1.5, as measured by an electroacoustic technique (ESA 9800, Matec Applied Science) on concentrated suspensions (ϕ_{micro} = 0.1). The Debye length (κ^{-1}) is 1.8 nm under the experimental conditions of interest (pH = 1.5).

Hydrous zirconia nanoparticles (Zr 10/20, Nyacol Products, Ashland, MA) served as the small colloidal species. The nanoparticles have an average radius, a_{nano}, of 3 nm, as determined by X-ray scattering measurements with a reported radius range of 0.5−11 nm.[25] Their reported density is 3.65 g/cm^3.[26,27] They are supplied in an acidic solution (pH = 0.5) at a volumetric solids loading of 7.4%. Due to the experimental limitations associated with small particle size and high ionic strength, zeta potential measurements could not be carried out. Therefore, we estimated the nanoparticle zeta potential to be on the order of 70 mV from their reported effective charge determined from titration studies[25] using the approach outlined by Gisler et al.[28]

Suspension Preparation. Concentrated colloidal suspensions were prepared by first adding an appropriate volume fraction of silica microspheres (ϕ_{micro} = 0.05−0.45) to deionized water. The suspensions were stirred for approximately 18 h with three intermittent sonications (model 550 sonic dismembrator, Fisher Scientific, Pittsburgh, PA) during the first 6 h. Nitric acid (reagant grade, Fisher Scientific) was then added to adjust the suspension pH to 1.5 ± 0.1. Each suspension was then resonicated followed by the addition of an appropriate volume fraction of nanoparticles ($\phi_{nano} = 10^{-6}-10^{-2}$). After the mixture was stirred for several hours, the suspension pH was readjusted to a value of 1.5 (if needed) and sonicated a final time. Each sonication step consisted of 5 pulsed min (1 s on/off) at 20 kHz.

Phase Behavior of Microsphere−Nanoparticle Mixtures. The phase behavior of binary mixtures of negligibly charged microspheres and highly charged nanoparticles was studied by observing concentrated mixtures (a_{micro} = 0.285 μm or 0.590 μm, ϕ_{micro} = 0.05−0.45 and varying ϕ_{nano}) during sedimentation. In these experiments, a given volume of each suspension was placed in a graduated cylinder (10 mL total volume), which was then capped to minimize solvent loss. Initially, these samples were opaque due to the scattering of visible light from the colloidal microspheres. As the microspheres settled, a clear supernatant formed above the sedimented region. A rich variety of phase behavior was observed including the formation of colloidal gels that could undergo further densification via sedimentation and a homogeneous (binary) fluid that settled to form an iridescent colloidal crystal.

Confocal Imaging of Microsphere−Nanoparticle Mixtures. Confocal microscopy (Multiprobe 2001, Molecular Dynamics) was used to study the structure of sedimented binary mixtures of varying composition. The samples were placed on the stage of an inverted Mikon Diaphot microscope equipped with a 514.5 nm argon laser source and 100× oil lens. Two-dimensional images were acquired as a function of layer depth, where the origin corresponded to the sediment−substrate interface. To determine the effects of stabilization mechanism on the structure of the assembled colloidal crystals, the average center-to-center distance between colloidal microspheres was calculated from a fast Fourier transform analysis of the acquired 2-D images. As a benchmark, suspensions of charge-stabilized microspheres were prepared in the absence of nanoparticles. Charge stabilization was achieved by tailoring solvent conditions (pH ∼ 6 and κ^{-1} = 9.6 nm) well away from the isoelectric point of silica. Such conditions simulated the effective charge buildup observed for silica microspheres in the presence of nanoparticles at pH = 1.5, albeit at lower ionic strength.[1]

Rheological Measurements. The flow properties of concentrated colloidal suspensions of fixed microsphere volume fraction (ϕ_{micro} = 0.3) and varying nanoparticle volume fraction ($\phi_{nano} = 0-10^{-2}$) were characterized using a Bohlin controlled stress rheometer (Bohlin Rheologi CVO, Cranbury, NJ) fitted with either a concentric cylinder (C25) or double concentric cylinder (DG24/27 or DG40/50) geometry. Their apparent viscosity (η_{app}) was measured as a function of ascending applied shear stress (τ). The measurements obtained using the Couette double-gap cell DG 24/27, which has a stress range of 0.004−477 Pa, are presented. Analogous measurements were also obtained using other cell geometries, suggesting that wall slip effects are negligible.[29]

The elastic (G') and storage (G'') moduli of concentrated colloidal suspensions of varying microsphere volume fractions (ϕ_{micro} = 0.3−0.45) and nanoparticle volume fractions ($\phi_{nano} = 0-10^{-2}$) were also characterized using a Bohlin controlled stress rheometer (Bohlin Rheologi CVO, Cranbury, NJ) fitted with a vane tool. The vane tool has a stress range of 0.02464−1232 Pa and a suitable geometry for these sensitive measurements.[30] Oscillatory measurements were carried out by first preshearing the mixtures at a rate of 400 s^{-1} for 600 s followed by a quiescent

(22) Garibay-Alonso, R.; Mendez-Alcaraz, J. M.; Klein, R. *Physica A* **1997**, *235*, 159−169.
(23) Ferreira, P. G.; Dymitrowksa, M.; Belloni, L. *J. Chem. Phys.* **2000**, *113*, 9849−9862.
(24) Mendez-Alcarez, J. M.; Klein, R. *Phys. Rev. E* **2000**, *61* (4), 4095−4099.
(25) Peyre, V.; Spalla, O.; Belloni, L.; Nabavi, M. *J. Colloid Interface Sci.* **1997**, *187*, 184−200.
(26) Miller, K. T.; Zukoski, C. F. *J. Am. Ceram. Soc.*, **1994**, *77*, 2473−2478.
(27) Flickinger, G. L. *The Gelation Behavior of Zirconia Sols*; University of Illinois: Urbana-Champaign, IL, 1997.
(28) Gisler, T.; Schulz, S. F.; Borkovec, M.; Sticher, H.; Schurtenberger, P.; D'Aguanno, B.; Klein, R. *J. Chem. Phys.* **1994**, *101*, 9924−9936.
(29) Buscall, R. *J. Rheol.* **1993**, *37*, 621−641.
(30) Nguyen, Q. D.; Boger, D. V. *J. Rheol.* **1983**, *27*, 321−349.

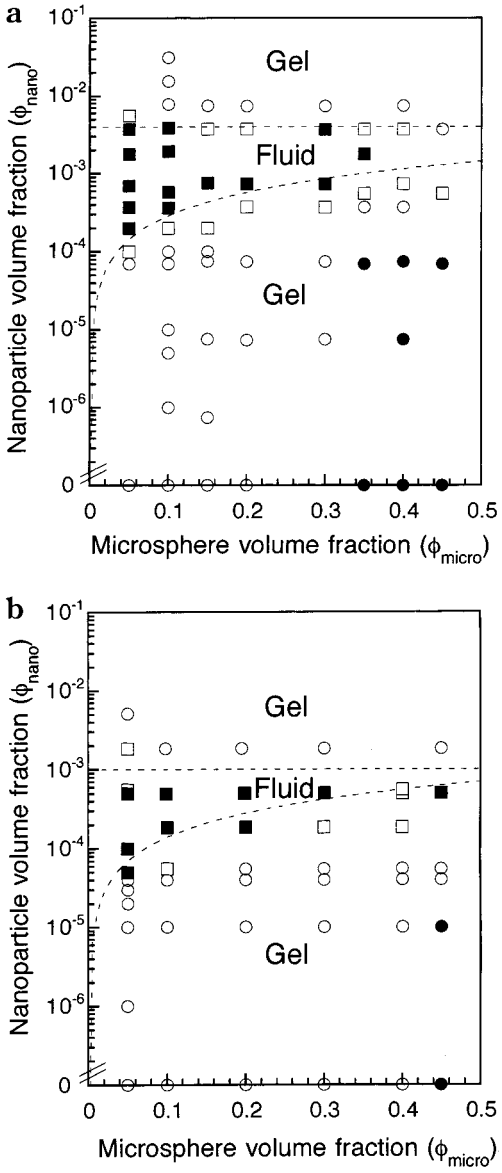

Figure 1. Semilog plots of the phase behavior of microsphere−nanoparticle mixtures of varying size ratio: (a) 95 and (b) 197. Open circles represent a weak colloidal gel and a nanoparticle fluid, filled circles represent a colloidal gel and nanoparticle fluid, filled squares represent a homogeneous fluid (*F*), and open squares represent samples which have separated into a homogeneous fluid and weak gel. The lower and upper dashed lines depict the experimentally observed lower ($\phi^{L,C}$) and upper ($\phi^{U,C}$) critical nanoparticle concentrations, respectively.

equilibration time of 2 h to minimize shear history effects.[31] The elastic (*G′*) and storage (*G″*) moduli were then measured by performing a stress sweep at a frequency of 1 Hz All measurements were done at 22 °C using a specially designed solvent trap filled with water to minimize evaporation. The reported values for the microsphere−nanoparticle mixtures correspond to those obtained at the lowest measurable strain (i.e., $\gamma = 0.00015$ in most cases).

Experimental Results

Phase Behavior of Microsphere−Nanoparticle Mixtures. Parts a and b of Figure 1 depict the phase behavior of microsphere−nanoparticle mixtures of varying composition and size ratios of 95 and 197, respectively. The phase diagrams for these two systems share several common features. In each case, the data presented delineates three regions: (a) a colloidal gel comprised of silica microspheres in coexistence with a nanoparticle fluid at nanoparticle volume fractions (ϕ_{nano}) below a lower critical value, $\phi^{L,C}$, (b) a homogeneous fluid comprised of stabilized silica microspheres and nanoparticles at intermediate nanoparticle volume fractions, $\phi^{L,C} \leq \phi_{nano} < \phi^{U,C}$, and (c) a colloidal gel comprised of silica microspheres in coexistence with a more concentrated nanoparticle fluid at nanoparticle volume fractions (ϕ_{nano}) above an upper critical value, $\phi^{U,C}$.

In the absence of nanoparticle species ($\phi_{nano} = 0$), both systems began in a nonequilibrium state. Negligibly charged silica spheres ($a_{micro} = 285$ and 590 nm) underwent rapid flocculation (∼seconds) to yield a colloidal gel. At $\phi_{micro} \leq 0.30$ ($a_{micro} = 285$ nm) and $\phi_{micro} \leq 0.40$ ($a_{micro} = 590$ nm), weak gels formed which settled quickly producing a loose-packed sediment and a clear supernatant. At higher respective values of ϕ_{micro}, stronger gels formed which could support their own mass and therefore did not undergo further densification in response to gravitational forces. Upon modest additions of nanoparticle species ($0 < \phi_{nano} < \phi^{L,C}$), each system remained in a nonequilibrium (gel) state. The silica microspheres flocculated in suspension to form a gel in coexistence with a nanoparticle fluid phase. Above a lower critical volume fraction ($\phi^{L,C}$) of nanoparticle species, a dramatic change in stability was observed. Many samples remained opaque for several days, until individual silica microspheres slowly settled yielding an iridescent,[32] colloidal crystal. Such samples, considered fully stabilized, are denoted by the homogeneous fluid phase in Figure 1. In each system, the value of $\phi^{L,C}$ increased with increasing microsphere volume fraction. However, for a given microsphere volume fraction, a lower value of $\phi^{L,C}$ was observed for mixtures of higher size ratio. Above the upper critical volume fraction ($\phi^{U,C}$) of nanoparticles, this dramatic change in stability was reversed. For $\phi_{nano} \geq \phi^{U,C}$, the silica microspheres again flocculated yielding a gel in coexistence with a nanoparticle fluid phase. Unlike the stabilizing transition, $\phi^{U,C}$ appears to exhibit little dependence on microsphere volume fraction for a given system. For example, $\phi^{U,C}$ was found to be approximately 0.004 and 0.001, respectively, for size ratios of 95 and 197. However, similar to $\phi^{L,C}$, a lower value of $\phi^{U,C}$ was needed for mixtures of higher size ratio.

Confocal Imaging of Microsphere−Nanoparticle Mixtures. Nanoparticle species strongly influence the structural evolution of phases formed under gravity-driven sedimentation. Microsphere−nanoparticle mixtures with compositions in the lower gel phase ($\phi_{nano} < \phi^{L,C}$) and in the homogeneous fluid phase ($\phi^{L,C} \leq \phi_{nano} < \phi^{U,C}$) were found to assemble under gravity to form colloidal gels and crystals, respectively, as shown in Figure 2. These representative images were selected because they provided the best clarity for comparing the structural features observed for these sedimented mixtures. Colloidal gels produced from binary mixtures were highly disordered structures, whose strength depended on both the microsphere and nanoparticle volume fractions. Iridescent colloidal crystals, assembled from homogeneous fluid phase (*F*) under gravity-driven sedimentation, consisted of a random stacking of close-packed layers. The average center-to-center distance (*D*) between the settled microspheres is plotted as a function of layer depth in Figure 3. Substrate (wall) interactions disrupt the layer structure at depths less than 3 μm[15,16,33] leading to a larger

(31) Rueb, C. J.; Zukoski, C. F. *J. Rheol.* **1997**, *41*, 197−218.

(32) Pusey, P. N.; van Megen, W. *Nature* **1986**, *320*, 340−342.

(33) Koenderink, G. H.; Vliegenthart, G. A.; Kluijtmans, G. J. M.; van Blaaderen, A.; Philipse, A. P.; Lekkerkerker, H. N. W. *Langmuir* **1999**, *15*, 4693−4696.

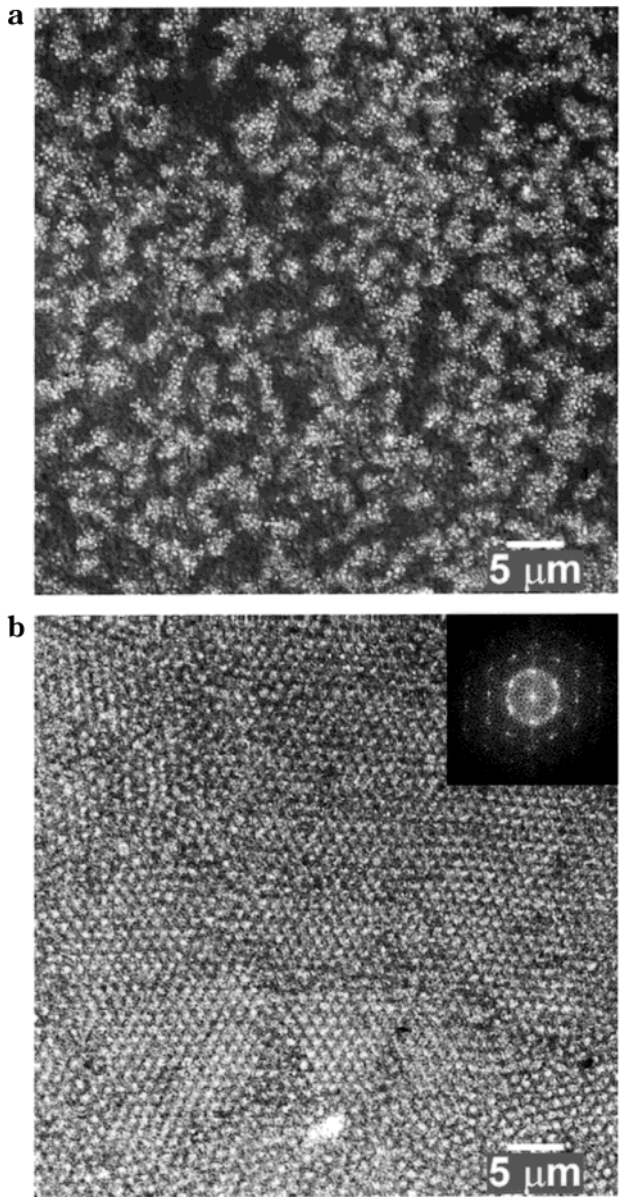

Figure 2. Confocal micrographs of representative sediment structures assembled under gravity: (a) colloidal gel (a_{micro} = 285 nm; $\phi_{micro} = 0.01$, $\phi_{nano} = 0$) and (b) colloidal crystal derived from the homogeneous fluid (*F*) phase (a_{micro} = 590 nm; ϕ_{micro} = 0.01, ϕ_{nano} = 0.000185). The inset in (b) is the fast Fourier transform (FFT) of the depicted image. Images are shown at different magnifications to highlight the structural features of interest.

separation distance. Deeper into the crystalline sediment, *D* exhibits a plateau value of 580 and 1180 nm, respectively, for fluids containing 570 ± 20 and 1180 ± 20 nm microspheres. These data strongly suggest that the microspheres assemble into a touching network, analogous to that expected for crystallized hard-sphere systems. In contrast, the benchmark system consisting of charge-stabilized silica microspheres exhibited an average center-to-center distance of roughly 7% higher than the nanoparticle-stabilized mixtures indicative of a more open spacing between colloidal particles in those assemblies.

Flow Behavior of Microsphere−Nanoparticle Mixtures. The flow behavior of microsphere−nanoparticle mixtures reflects the profound structural variations in the phases described above. The apparent viscosities as a function of shear rate for microsphere−nanoparticle mixtures with a size ratio of 95 are shown in Figure 4. In

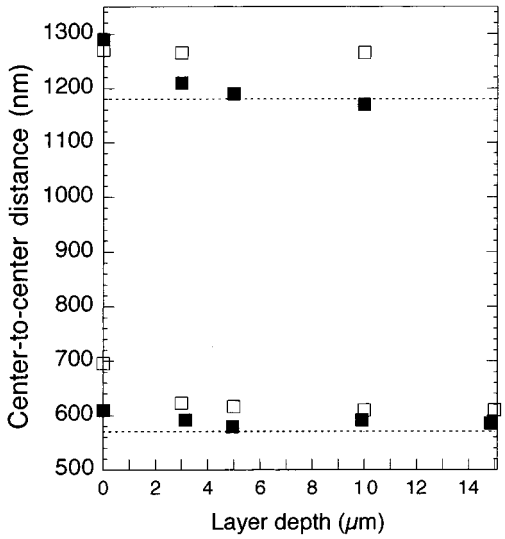

Figure 3. Average center-to-center separation distance (*D*) between microspheres as a function of layer depth from the sediment−substrate interface. The dashed lines correspond to respective measured diameters ($2a_{micro}$) for microspheres of a_{micro} = 285 nm and a_{micro} = 590 nm. Colloidal crystals were assembled under gravity-driven sedimentation from nanoparticle-stabilized microspheres (filled symbols; $\phi_{micro} = 0.01$, $\phi_{nano} = 1.85 \times 10^{-3}$, a_{micro} = 285 nm, and $\phi_{micro} = 0.01$, $\phi_{nano} = 1.85 \times 10^{-4}$; a_{micro} = 590 nm) at pH = 1.5, κ^{-1} = 1.8 nm and from charge-stabilized microspheres ($\phi_{micro} = 0.01$, $\phi_{nano} = 0$) at pH ∼ 5.5, κ^{-1} = 9.8 nm with a $\zeta = -60$ mV, which is comparable in magnitude to that observed for the "nanoparticle-haloed" microspheres.[1]

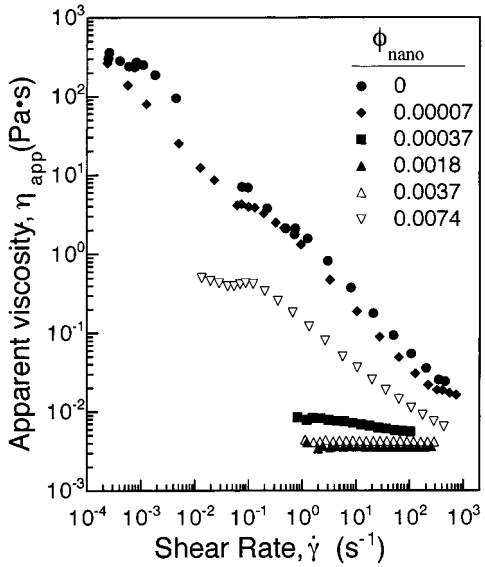

Figure 4. log−log plot of apparent viscosity (η_{app}) as a function of shear rate ($\dot{\gamma}$) for microsphere−nanoparticle mixtures at constant microsphere volume fraction (ϕ_{micro} = 0.30 and a_{micro} = 285 nm) and varying nanoparticle volume fraction (ϕ_{nano}).

the absence of nanoparticles, the pure microsphere suspension exhibited a low shear viscosity of roughly 400 Pa•s and strong shear thinning behavior characteristic of a flocculated system. Both the viscosity and degree of shear thinning decreased dramatically with increasing nanoparticle volume fraction. Suspensions prepared within the homogeneous fluid phase (*F*), where $\phi^{L,C} \leq \phi_{nano} < \phi^{U,C}$, exhibited an apparent viscosity of ∼0.004 Pa•s, several orders of magnitude less than the flocculated systems. As expected, these fully stabilized suspensions also exhibited Newtonian flow behavior. At $\phi_{nano} \geq \phi^{U,C}$, the mixtures reflocculated as evidenced by increases in their apparent

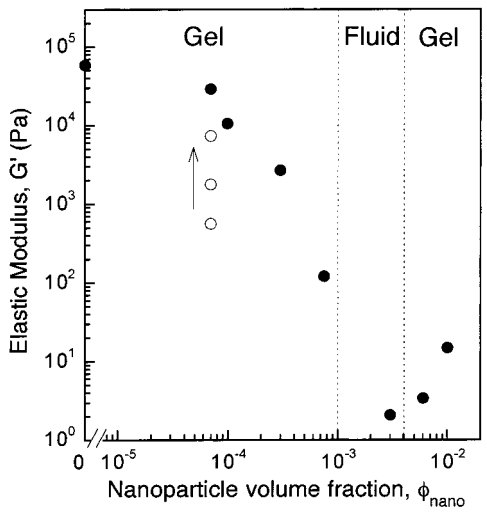

Figure 5. log−log plot of elastic modulus (G') of microsphere−nanoparticle mixtures as a function of nanoparticle volume fraction (ϕ_{nano}) at a constant microsphere volume fraction ($\phi_{micro} = 0.45$ and $a_{micro} = 285$ nm, filled symbols). Dashed lines denote the boundaries between the lower gel, fluid, and upper gel phase regions shown in Figure 1a for such mixtures. The open symbols depict the dependence of G' on microsphere volume fraction (ϕ_{micro}) for mixtures of constant nanoparticle volume fraction ($\phi_{nano} = 7 \times 10^{-5}$). The arrow denotes the direction of increasing ϕ_{micro}, which ranges from 0.3 to 0.45 in increments of 0.05.

viscosity and degree of shear thinning. For example, when ϕ_{nano} was increased to nearly double the value of $\phi^{U,C}$, the low shear suspension viscosity was 2 orders of magnitude higher than that observed for the fully stabilized suspensions (F).

Oscillatory measurements were carried out on microsphere−nanoparticle mixtures residing in the lower gel ($\phi_{nano} < \phi^{L,C}$), fluid ($\phi^{L,C} \leq \phi_{nano} < \phi^{U,C}$), and upper gel ($\phi_{nano} \geq \phi^{U,C}$) phase regions. The elastic modulus (G') of mixtures of fixed microsphere volume fraction ($\phi_{micro} = 0.45$) displayed a strong dependence on nanoparticle volume fraction (ϕ_{nano}), as shown in Figure 5. The dashed lines denote the observed boundaries between the three phases based on the data for $\phi_{micro} = 0.45$ shown in Figure 1a. In the absence of nanoparticles, concentrated microsphere gels exhibited a G' of 50000−60000 Pa. Within the lower gel phase, the value of G' decreased more than 3 orders of magnitude as ϕ_{nano} approached $\phi^{L,C}$. In contrast, mixtures residing in the upper gel phase exhibited the opposite dependence of G' on ϕ_{nano}. In this region, G' was observed to gradually increase as ϕ_{nano} increased beyond $\phi^{U,C}$. As expected, microsphere−nanoparticle mixtures residing in the homogeneous fluid phase exhibited the lowest values of G' on the order of a few pascals. For comparison, the elastic modulus (G') of gels of fixed nanoparticle volume fraction ($\phi_{nano} = 7 \times 10^{-5} < \phi^{L,C}$) and varying microsphere volume fraction (ϕ_{micro}) are also shown in Figure 5. The arrow illustrates the direction of increasing ϕ_{micro}, which ranges from 0.3 to 0.45 in increments of 0.05. These data (open symbols) clearly show that G' increases with increasing microsphere volume fraction. A power law dependence of $G' \sim \phi^{9.7}$ was observed far exceeding the power law exponents ($m \sim 4-5$) reported for other colloidal gels.[31,34] We believe this difference reflects the fact that systems of fixed nanoparticle volume fraction experience differences in both bond density *and* strength with increasing ϕ_{micro}. Such mixtures become less stable with increasing microsphere volume fraction due to the increased microsphere surface area that must be decorated by nanoparticle halos. Therefore, their stronger power law dependence seems reasonable given that previous studies have determined this type of scaling behavior solely for colloidal gels with fixed interparticle interactions (or bond strength).

Discussion

Modeling of Colloidal Interactions. Colloidal stability is governed by the total interparticle interaction energy (V_{total}) at a given interparticle separation distance, h. Important contributions for the experimental system of interest include

$$V_{total}(h) = V_{vdW}(h) + V_{el}(h) + V_{dep}(h) \quad (1)$$

where $V_{vdW}(h)$ is an attractive potential arising from long-range van der Waals forces (vdW) between particles, $V_{el}(h)$ is a repulsive potential due to electrostatic forces between particles, and $V_{dep}(h)$ is the depletion potential arising from the presence of nanoparticle species in solution.

The first two terms of eq 1 constitute the well-known DLVO (Derjaguin−Landau−Verwey−Overbeek) theory.[35,36] The attractive van der Waals (vdW) dispersion forces arise when dipoles interact across an intervening medium. The vdW potential ($V_{vdW}(h)$) between two identical, spherical particles of radius a is given by

$$V_{vdW}(h) = \frac{-A_{131}(h)}{6}\left[\frac{2}{s^2-4} + \frac{2}{s^2} + \ln\left(\frac{s^2-4}{s^2}\right)\right] \quad (2)$$

where

$$s = \frac{2a + h}{a}$$

and $A_{131}(h)$ is the distant-dependent Hamaker value. Electrostatic forces give rise to repulsive interactions between like-charged colloidal particles suspended in a polar solvent. If one assumes a constant, low potential on the particles and a relatively thin double layer, the repulsive electrostatic potential between two spheres of equal radius, a, and surface potential, ψ_0, is given by[36]

$$V_{el}(h) = 2\pi\epsilon\epsilon_0 a\psi_0^2 \ln(1 + \exp(-\kappa h)) \quad (3)$$

where ϵ is the relative permittivity of the solution, ϵ_0 is the permittivity of vacuum, κ^{-1} is the Debye length, and h is the surface separation distance. In the following calculations, the zeta potential is substituted for ψ_0.[37]

DLVO potential energy curves were calculated for microsphere−microsphere interactions using eqs 1−3 and distant-dependent Hamaker values, $A_{131}(h)$ (see Appendix A) for the experimental conditions of interest (pH = 1.5 and $\zeta_{micro} = 1$ mV). These curves are shown in parts a and b of Figure 6 for silica microspheres of radius 285 and 590 nm, respectively. In the absence of nanoparticle additions, van der Waals forces dominated the microsphere−microsphere interactions, as reflected by a primary attractive minimum (see curve A in Figure 6) whose depth at a given separation distance increased with increasing microsphere

(34) Buscall, R.; Mills, P. D.; Goodwin, J. W.; Lawson, D. W. *J. Chem. Soc., Faraday Trans. 1* **1988**, *84*, 4249−4260.

(35) Israelachvili, J. *Intermolecular & Surface Forces*, 2nd ed.; Academic Press: London, 1991.

(36) Hunter, R. J. *Foundations of Colloid Science*; Claredon Press: Oxford 1995; Vols. 1 & 2.

(37) Overbeek, J. T. G. *J. Colloid Interface Sci.* **1977**, *58*, 408−422.

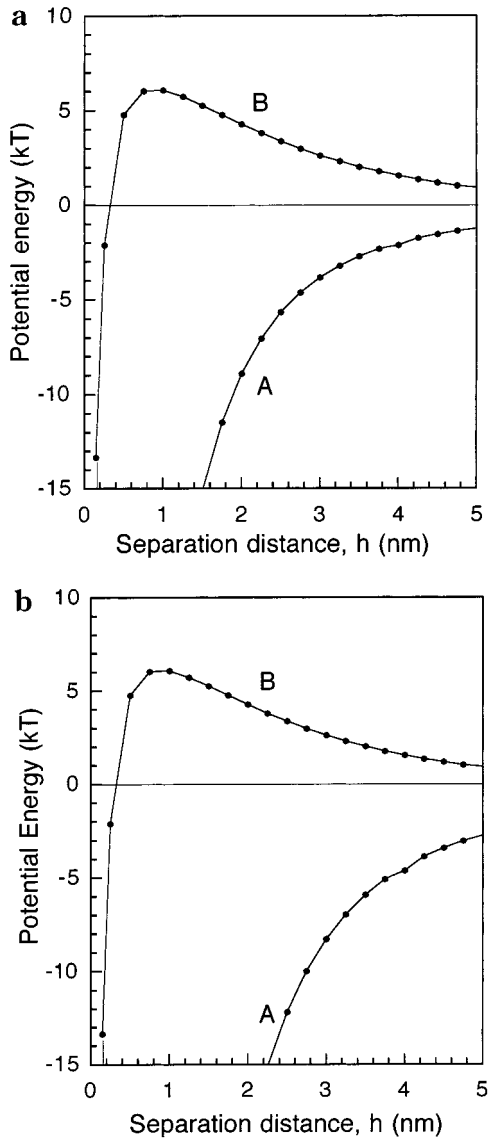

Figure 6. Calculated potential energy of interaction (DLVO model) as a function of interaparticle separation distance between microspheres (curve A) of radius, a_{micro} (a) 285 nm and (b) 590 nm and nanoparticles (curve B) of radius, a_{nano}, 3 nm at pH = 1.5.

radius. DLVO potential energy curves were also calculated for the nanoparticle−nanoparticle interactions using eqs 1−3 and the distant-dependent Hamaker values $A_{232}(h)$ (see Appendix A) for the experimental conditions of interest (pH = 1.5 and an estimated ζ_{nano} = 70 mV). These data, represented by curve B, are plotted alongside curve A in Figure 6. The interactions between highly charged nanoparticles exhibited a long-range repulsion stemming from electrostatic interactions with a maximum barrier height of ~5 kT. The estimated effective nanoparticle radius, a_{nano}^{eff}, of 5−8 nm is in good agreement with these data.[38] Note, there is likely some error for these nanoparticle pair potential calculations since the appropriate parameters lie outside of the valid range of conditions for eq 3.

The self-organization of highly charged nanoparticles in solution can give rise to additional interactions between suspended microspheres stemming from nanoparticle haloing[1] and depletion[18−21] effects. Nanoparticle haloing describes the segregation of highly charged nanoparticles to regions near negligibly charged colloidal microspheres, as predicted by Garibay-Alonso et al.[22] and observed experimentally by Lewis and co-workers.[1] This process can be driven solely by repulsive interactions between such species in solution but would be further enhanced by a weak attraction between the microspheres and nanoparticles, such as may arise from long-range van der Waals or locally induced electrostatic interactions.[39,40] Recently, we have shown that silica microspheres suspended at pH = 1.5 (near their isoelectric point) adopt an effective charge (ζ_{micro}) of ~65 mV with increasing nanoparticle volume fraction in solution. This plateau value is in remarkable agreement with the estimated ζ_{nano} of the decorating nanoparticle species. As a result of this effective charge buildup, the interactions between two colloidal microspheres would now be dominated by a long-range repulsion leading to their observed stability above a lower critical nanoparticle volume fraction ($\phi^{L,C}$). In the simplest case, one could view this repulsion to be of the magnitude and range depicted by curve B in Figure 6. A more accurate model of the microsphere−microsphere pair potential in the presence of nanoparticle species, however, must account for van der Waals interactions between microspheres as well as the exact spatial distribution and charge of the nanoparticle species surrounding the microspheres and those effects on the resulting electrostatic potential. This type of modeling is beyond the present scope; however it is a subject of future interest.

As the nanoparticle volume fraction in solution increases, one must also account for depletion effects. While several theories[18−21,41−46] have been developed, the model by Walz and Sharma[21] (WS) is most appropriate for our system because it can treat the intensified interactions stemming from charged nanoparticle species. The WS model[21] uses a second-order virial expansion to account for depletant−depletant and depletant−colloid interactions for interparticle distances up to $h < 4a_{dep}$. By use of this model, the depletion interaction potential energy between two silica microspheres was calculated by Piech and Walz[47] as a function of varying nanoparticle volume fraction. The data obtained for microspheres of radii 285 and 590 nm are shown in parts a and b of Figure 7, respectively. For the range of nanoparticle volume fractions studied, their calculations predicted only a first-order depletion attraction whose strength increased with increasing microsphere-to-nanoparticle size ratio and nanoparticle volume fraction. For microsphere−nanoparticle mixtures of smaller size asymmetry (a_{micro} = 285 nm), a first-order depletion attractive potential of roughly −3 kT was calculated for ϕ_{nano} = 0.004. For binary mixtures of larger size asymmetry (a_{micro} = 590 nm), their calculations indicate that an attractive potential of similar magnitude would occur at $\phi_{nano} \sim 0.001$. Depletion effects therefore only account for the observed microsphere reflocculation at $\phi^{U,C}$, not the remarkable stabilization at lower nanoparticle volume fractions.

(38) Tohver, V. Phase Behavior, Structure, and Properties of Colloidal Microsphere-Nanoparticle Mixtures. Ph.D. Thesis, University of Illinois, Urbana-Champaign, IL, 2001.

(39) Miklavic, S. J., Chan, D. Y. C.; White, L. R. *J. Phys. Chem.* **1994**, *98*, 9022−32.
(40) Spalla, O.; Belloni, L. *Phys. Rev. Lett.* **1995**, *74*, 2515−2518.
(41) Vrij, A. *Pure Appl. Chem.* **1976**, *48*, 471−483.
(42) Joanny, J. F.; Leibler, L.; de Gennes, P. G. *J. Polym. Sci., Polym. Phys. Ed.* **1979**, *17*, 1073−1084.
(43) Chatterjee, A. P.; Schweizer, K. S. *J. Chem. Phys.* **1998**, *109*, 10464−10476.
(44) Chatterjee, A. P.; Schweizer, K. S. *J. Chem. Phys.* **1998**, *109*, 10477−10488.
(45) Rosenfeld, Y. *Phys. Rev. Lett.* **1994**, *72*, 3831−3834.
(46) Chu, X. L.; Nikolov, A. D.; Wasan, D. T. *Langmuir* **1996**, *12*, 5004−5010.
(47) Piech, M., Walz, J. Y. Unpublished data.

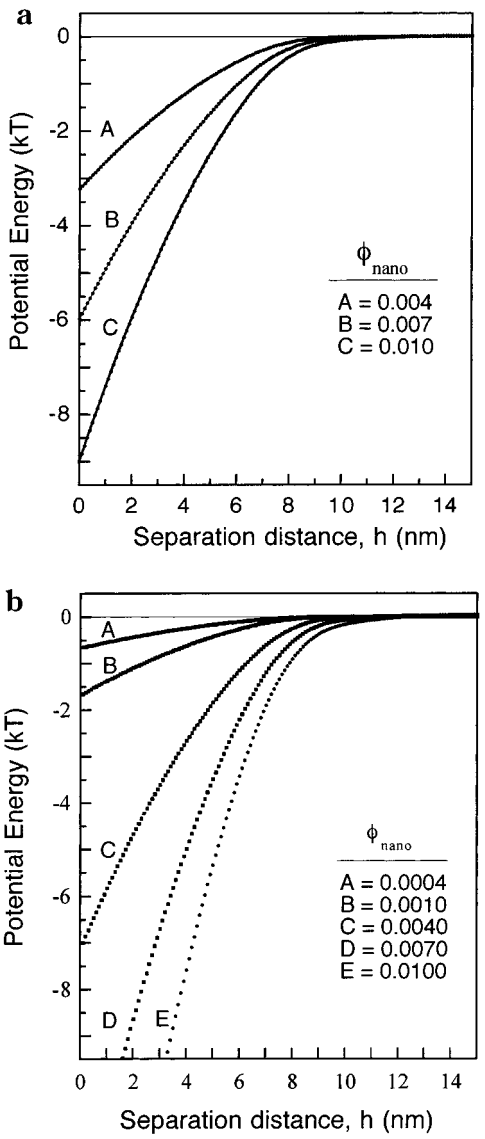

Figure 7. Calculated potential energy of interaction (WS depletion model) as a function of interparticle separation distance between microspheres of radius, a_{micro} (a) 285 nm and (b) 590 nm suspended in solutions of varying nanoparticle volume fraction (ϕ_{nano}).

Nanoparticle Engineering of Binary Mixture Behavior. The phase behavior, structure, and flow properties of these microsphere−nanoparticle mixtures are governed by the colloidal interactions outlined above. As stated previously, several phases were observed including a colloidal gel in coexistence with a nanoparticle fluid when $\phi_{nano} < \phi^{L,C}$, a homogeneous (binary) fluid when $\phi^{L,C} \leq \phi_{nano} < \phi^{U,C}$, and a colloidal gel in coexistence with a more concentrated nanoparticle fluid when $\phi_{nano} \geq \phi^{U,C}$. The stabilizing transition that occurs for nanoparticle volume fractions above $\phi^{L,C}$ arises from nanoparticle haloing effects.[1] Our newly discovered approach of using highly charged nanoparticles to regulate the charge of primary colloidal particles contrasts sharply with the traditional approach of tailoring solvent pH well away from their isoelectric point.[36] Yet, we have presented strong evidence that otherwise attractive colloidal microspheres can be fully stabilized by this method. The most compelling observation is that binary mixtures prepared within the homogeneous fluid (*F*) phase assembled into close-packed colloidal arrays under gravity-driven sedimentation. Additionally, such mixtures exhibited low apparent viscosities and Newtonian flow behavior. Finally, Tohver et al.[1] have also directly imaged discrete silica microspheres suspended in such mixtures using optical microscopy.

The origin of microsphere reflocculation at nanoparticle volume fractions above $\phi^{U,C}$ is explained by the rigorous force-balance depletion (WS) model.[21] Flocculation of colloidal systems generally requires an attractive interaction of a few kT in magnitude. As stated above, an attractive depletion potential of roughly -3 kT was calculated $\phi_{nano} = 0.004$ and $\sim$0.001 for systems of size ratio equal to 95 and 197, respectively.[47] These respective values corresponded to the $\phi^{U,C}$ values depicted by the upper dashed line in parts a and b of Figure 1, respectively, and are in excellent agreement with our experimental observations.

By tailoring the strength of energetic and entropic forces through nanoparticle engineering, one can substantially vary the structure and flow properties of binary mixtures within a given phase region. We begin by examining compositional effects on the behavior of the lower and upper gel phases. As nonequilibrium structures, gels can evolve over time depending on the stresses and thermal motions of particles within the network. Their resistance to particle rearrangement is governed by the interparticle bond density and strength. The elastic modulus is a good figure of merit that describes the gel strength. For both the lower and upper gel regions, the gel strength was found to increase with increasing microsphere additions at a fixed nanoparticle volume fraction (e.g., see Figure 5). This trend reflects the enhanced bond density within the gel as ϕ_{micro} increases. Subtle variations in bond strength are also expected for these mixtures, since the extent of nanoparticle haloing (i.e., $\phi^{L,C}$) depends on ϕ_{micro}.

For binary mixtures of constant microsphere volume fraction, we observed opposite dependencies of gel strength on nanoparticle volume fraction for the lower and upper gel phases. In the lower gel region ($\phi_{nano} < \phi^{L,C}$), the gel strength was found to decrease substantially with increasing nanoparticle volume fraction as a result of nanoparticle haloing, which mitigates the long-range van der Waals interactions between microspheres. This trend is clearly illustrated by the G' data in Figure 5 as well as in viscosity data shown in Figure 4. Here, the dominant effect of nanoparticle additions is to enhance the effective charge buildup on the colloidal microspheres.[1] Because nanoparticle stabilization occurs at such low volume fractions, depletion effects are negligible for this compositional range (see Figure 7). In sharp contrast, the gel strength was found to increase with increasing nanoparticle additions in the upper gel region ($\phi_{nano} \geq \phi^{U,C}$). Because the effective charge buildup on the microsphere surfaces has already reached a plateau value in this phase region, additional nanoparticle species merely serve to intensify attractive depletion interactions between the microspheres. Therefore, one can regulate the structure and, hence, mechanical properties of both of these gel phases simply by tuning the strength of interparticle interactions through compositional modulations.

Complete stabilization was achieved at intermediate nanoparticle volume fractions ($\phi^{L,C} < \phi_{nano} < \phi^{U,C}$) leading to the formation of close-packed colloidal arrays under gravity-driven sedimentation. Above $\phi^{L,C}$ at a given microsphere volume fraction, one expects enhanced osmotic consolidation of these ordered microsphere domains to ensue as ϕ_{nano} approaches $\phi^{U,C}$, i.e., as depletion attraction increases for these mixtures. As shown in Figure 3, the nanoparticle-stabilized microspheres assembled under gravity to yield close-packed colloidal arrays with a center-to-center separation distance between micro-

spheres of roughly $2a_{micro}$. In contrast, close-packed colloidal arrays assembled from charge-stabilized microspheres displayed a more open structure, with a center-to-center separation distance approximately 7% higher. Direct comparison of these data is complicated by differences in the κ^{-1} values between the two systems. An identical value of κ^{-1} could not be generated for charge-stabilized microspheres in the absence of nanoparticle species, while still maintaining the desired colloidal stability required for crystallization. We therefore selected a value ($\kappa^{-1} = 9.6$ nm) used for the charge-stabilized samples that was nearly equivalent to $2(a_{nano} + \kappa^{-1})$, where $\kappa^{-1} = 1.8$ nm for the nanoparticle-stabilized system. The observed differences in particle packing have important implications on the ability to harvest colloidal crystals from solution without the formation of drying-induced defects (i.e., cracks).[48] Further work is necessary to systematically study the effects of varying microsphere and nanoparticle volume fractions on the structure of colloidal crystals assembled from the homogeneous fluid phase (F). However, in an analogous fashion to the more pronounced effects observed for the gel phase, we anticipate that subtle variations in D will arise as composition is varied. Such effects may broadly impact the development of 3-D photonic band gap materials, whose properties are governed by defect states present in these periodic colloid-based structures.[7,8,49]

Conclusions

We have studied the phase behavior, structure, and rheological properties of binary mixtures of colloidal microspheres and highly charged nanoparticles that exhibit significant deviations from hard-sphere behavior. We showed that both energetic and entropic considerations play an important role in governing the behavior of such complex systems. By exploiting these interactions through compositional modulation, we fabricated colloidal gels of varying strength whose attractive interactions were dominated either by long-range van der Waals forces or tunable depletion forces as well as robust colloidal crystals. Nanoparticle engineering of colloidal stability is not limited to systems of low pH, such as the one studied here. The salient feature of our approach is that the colloidal microspheres are negligibly charged (be they suspended near their isoelectric point or surface functionalized with appropriate neutral groups) while the nanoparticles are highly charged (either positively or negatively) under the pH conditions of interest. The observed phenomena are therefore likely to be quite general and, thus, have important implications for self-assembly of materials,[50,51] adaptive fluids,[52] and, perhaps even, protein crystallization.[53,54]

Acknowledgment. We thank P. Wiltzius for help with confocal measurements, M. Piech and J. Walz for help with depletion calculations, and C. Martinez for help with the manuscript preparation. We also thank K. Schweizer, S. Granick, K. Suslick, C. Zukoski, and P. Braun for fruitful discussions. This work was supported by the NASA Microgravity Research Program (NAG8-1471).

Appendix A. Hamaker Function $A_{ijk}(h)$

The distant-dependent Hamaker constant was calculated using the approach of Prieve and Russel,[55] which accounts for the effects of retardation and high ionic strength through the following set of equations:

$$\frac{A_{132}(h)}{kT} = \frac{3(\epsilon_{10} - \epsilon_{30})(\epsilon_{20} - \epsilon_{30})}{4(\epsilon_{10} + \epsilon_{30})(\epsilon_{20} + \epsilon_{30})}(1 + 2\kappa h)\exp(-2\kappa h) + \frac{3}{2}\sum_{n=1}^{\infty}\Delta_{13}^{*}\Delta_{23}^{*}(r_n + 1)e^{-r_n}$$

$$\epsilon_j = \begin{cases} 1 + C_j/(1 + (\xi_n/\omega_j)^2) & \text{for } \xi_n > 0 \\ \epsilon_{j0} & \text{for } \xi_n = 0 \end{cases} \quad \text{(A.1)}$$

$$\Delta_{jk}^{*}(i\xi_n) = \frac{\epsilon_j(i\xi_n) - \epsilon_k(i\xi_n)}{\epsilon_j(i\xi_n) + \epsilon_k(i\xi_n)}$$

$$r_n = 2h\xi_n\epsilon_3^{1/2}/c$$

$$\xi_n = 2\pi nkT/\hbar$$

where kT is the thermal energy, ϵ_{j0} is the static dielectric for material k ($k = 1$ or 2) or solvent ($k = 3$), $1/\kappa$ is the Debye screening length, h is the surface−surface separation distance, ϵ_j is the frequency-dependent dielectric constant approximated by the value C_j at a characteristic absorption peak value, ω_j, and $\hbar$ is Planck's constant. This equation was specifically used to determine the distant-dependent Hamaker constant between like surfaces at pH = 1.5 where $[HNO_3] = 0.03$ M.

Due to both the complexity of including multiple dielectric constants for the IR range for water and its minor contribution to the distant-dependent Hamaker constant at small separations, the dielectric response of the material was represented by a single UV relaxation term. All values reported in Table 1 are taken from the literature.[56−58] Dielectric data for hydrous zirconia was not available, we therefore utilized values reported for tetragonal zirconia for these calculations.

Table 1. Material Spectral Parameters

material	ϵ_0	C_{UV}	ω_{UV} ($\times 10^{16}$) rad/s	n
fused silica	3.8	1.098	2.033	1.45
zirconia	18	3.74	1.34	
water	79.69	0.762	1.992	1.33

LA011252W

(48) Guo, J. J.; Lewis, J. A. *J. Am. Ceram. Soc.* **1999**, *82*, 2345−2358.
(49) Biswas, R.; Sigalas, M. M.; Subramania, G.; Ho, K.-M. *Phys. Rev. B* **1998**, *57*, 3701−3705.
(50) Dinsmore, A. D.; Crocker, J. C.; Yodh, A. G. *Curr. Opin. Colloid Interface Sci.* **1996**, *3*, 5−11.
(51) Alexander, S.; Chaikan, P. M.; Grant, P.; Morales, G. J.; Pincus, P.; Hone, D. *J. Chem. Phys.* **1984**, *80*, 5776−5781.
(52) Beebe, D. J.; Moore, J. S.; Bauer, J. M.; Yu, Q.; Liu, R. H.; Devadoss, C.; Jo, B.-H. *Nature* **2000**, *404*, 588−590.
(53) Rosenbaum, D.; Zamora, P. C.; Zukoski, C. F. *Phys. Rev. Lett.* **1996**, *76*, 150−153.
(54) ten Wolde, P. R.; Frenkel, D. *Science* **1997**, *277*, 1975−1978.
(55) Prieve, D. C.; Russel, W. B. J. *Colloid Interface Sci.* **1988**, *125*, 1−13.
(56) *CRC Handbook of Chemistry and Physics*, 71st ed.; CRC Press: Boca Raton, FL, 1990.
(57) Hough, D. B.; White, L. R. *Adv. Colloid Interface Sci.* **1980**, *14*, 3−41.
(58) Bergstrom, L.; Meurk, A.; Arwin, H.; Rowcliffe, D. J. *J. Am. Ceram. Soc.* **1996**, *79*, 339−348.